nature cell biology

DOI: 10.1038/ncb3518

In the format provided by the authors and unedited.

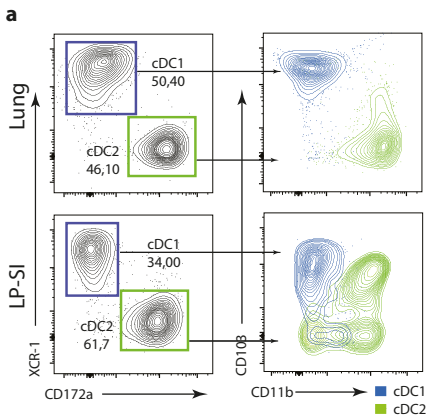

Supplementary Figure 1 CD103 and CD11b expression in cDC1s (blue) and cDC2s (green) from lung and LP-SI **(a).**

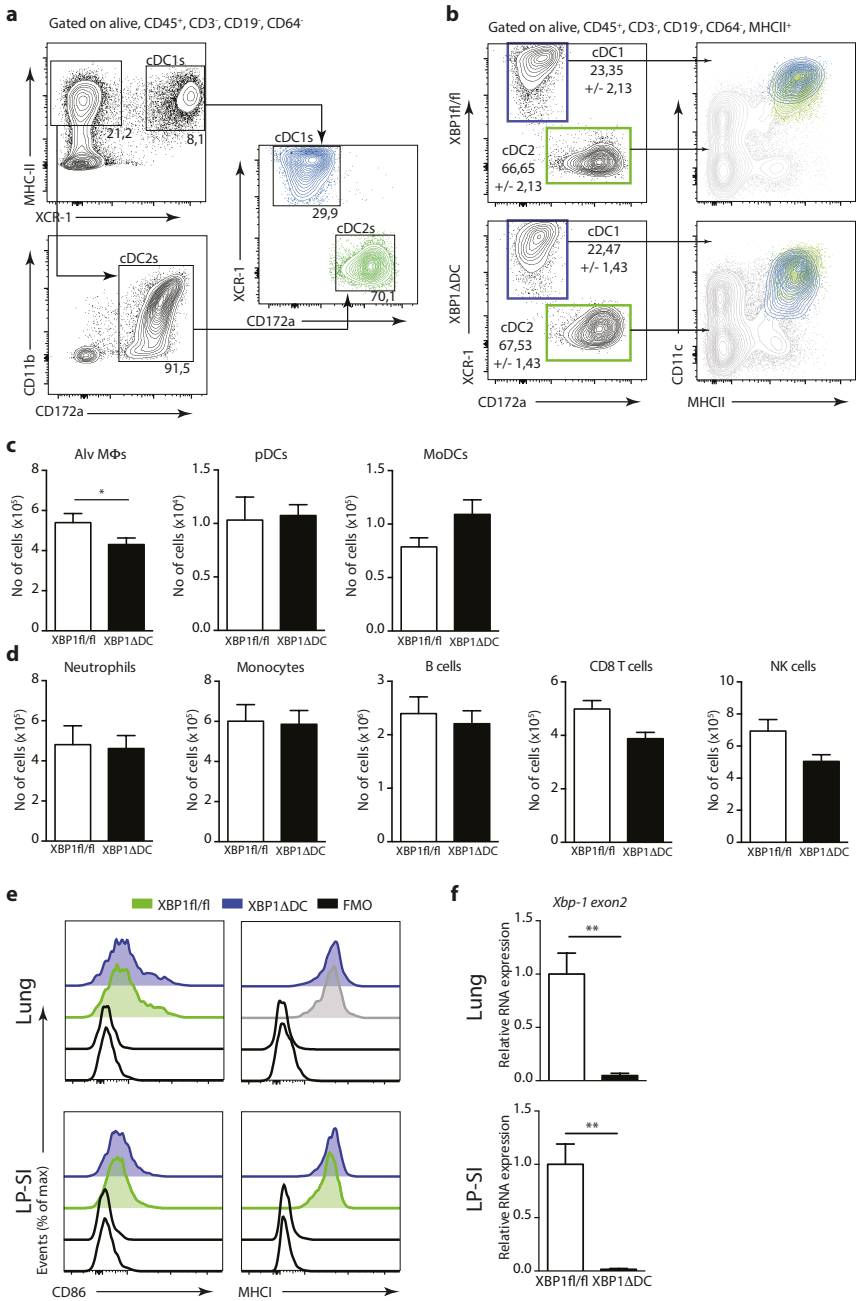

Supplementary Figure 2 XBP1 deletion affects mucosal cDCs differentially. **a,** cDC gating strategy independently of the integrin CD11c. **b,** cDC1 and cDC2 distribution in the spleen of *Xbp1*$^{fl/fl}$ (n=6 mice) and XBP1ΔDC mice (n=8 mice) (left plots) and their respective CD11c and MHCII expression (right plots: cDC1s - blue/cDC2s - green/CD45^{+}, Lin^{-}, CD64^{-} cells - grey). Data shows mean +/- S.E.M. **c,** number of alveolar macrophages ($n^{Xbp1fl/fl}$=12 mice, $n^{XBP1\Delta DC}$=14 mice), plasmacytoid DCs ($n^{Xbp1fl/fl}$=5 mice, $n^{XBP1\Delta DC}$=8 mice) and monocyte DCs ($n^{Xbp1fl/fl}$=12 mice, $n^{XBP1\Delta DC}$=14 mice) in the lungs of *Xbp1*$^{fl/fl}$ and XBP1ΔDC mice. P=0,0173, Mann-Whitney Test. Bar graphs represent mean +/- S.E.M. **d,** number of neutrophils ($n^{Xbp1fl/fl}$=10 mice, $n^{XBP1\Delta DC}$=12 mice), monocytes ($n^{Xbp1fl/fl}$=10 mice, $n^{XBP1\Delta DC}$=12 mice), B-cells ($n^{Xbp1fl/fl}$=12 mice, $n^{XBP1\Delta DC}$=14 mice), CD8 T-cells ($n^{Xbp1fl/fl}$=5 mice, $n^{XBP1\Delta DC}$=8 mice) and NK cells ($n^{Xbp1fl/fl}$=5 mice, $n^{XBP1\Delta DC}$=8 mice) in the lungs of *Xbp1*$^{fl/fl}$ and XBP1ΔDC mice. Bar graphs represent mean +/- S.E.M. **e,** expression of CD86 and MHCI in lung and intestinal cDC1s from *Xbp1*$^{fl/fl}$ and XBP1ΔDC mice. Fluorescence minus one (FMO) from both *Xbp1*$^{fl/fl}$ and XBP1ΔDC cDC1s are depicted as controls. **f,** RT-qPCR analysis of *Xbp1 exon2* mRNA among total mRNA prepared from sorted lung ($n^{Xbp1fl/fl}$=12 mice, $n^{XBP1\Delta DC}$6 mice) and LP-SI cDC1s ($n^{Xbp1fl/fl}$=7 mice, $n^{XBP1\Delta DC}$=6 mice). Results are normalized to *gapdh* and *ywhaz*. Bar graphs show mean +/- S.E.M. $P^{(lung)}$=0,0039, $P^{(LP-SI)}$=0,0002, Unpaired Student T-test. Data are pooled across 2 (c-f) similar experiment or representative of at least 3 (a,b) independent experiments.

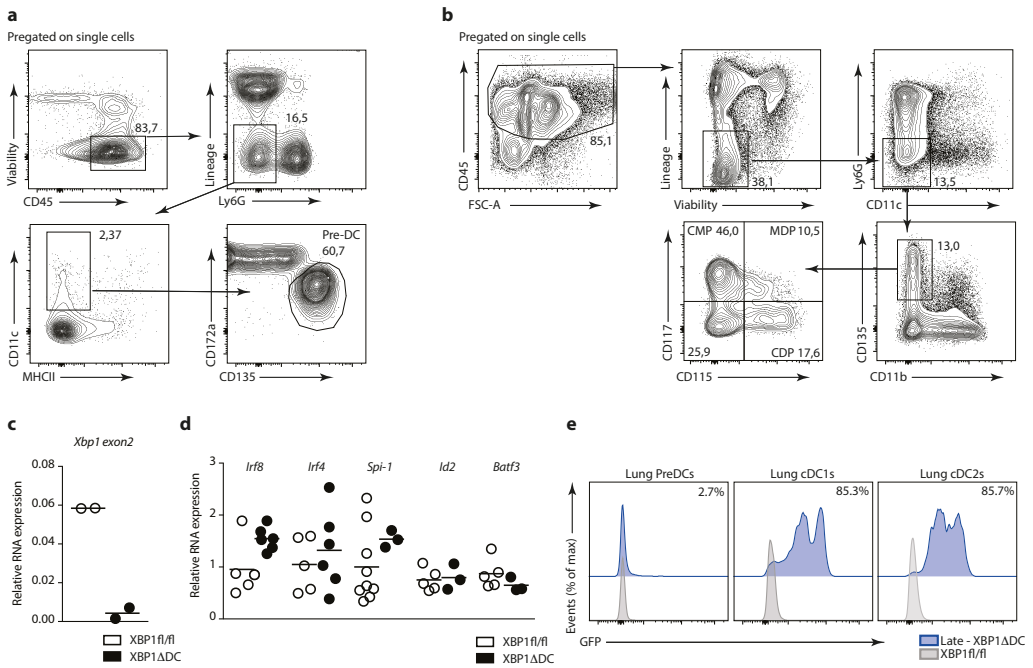

Supplementary Figure 3 XBP1 deficient cDC1s develop normally. **a,** gating strategy for defining pre-DCs in BM, spleen, lung and LP-SI. Numbers in graphs represent percentage of cells of one representative sample. **b,** applied gating strategy for defining Flt3$^+$ DC progenitors in BM. Numbers in graphs represent percentage of cells of one representative sample. **c,** RT-qPCR analysis of *Xbp1* in BM derived preDCs from XBP1$^{fl/fl}$ or XBP1ΔDC mice cultured for 12h with Flt3L; results are normalized to *gapdh*. Bar graphs depict mean +/- S.E.M. (n=2). **b,** Quantitative real-time PCR analysis of genes involved in cDC development among total RNA prepared from sorted cDC1s of lung and LP-SI; results are normalized to *gapdh* and *ywhaz*. Bar graphs depict mean +/- S.E.M. *Irf8, Irf4* ($n^{Xbp1fl/fl}$=5 mice, $n^{XBP1\Delta DC}$=6 mice), *Spi1* ($n^{Xbp1fl/fl}$=8 mice, $n^{XBP1\Delta DC}$=3 mice), *Id2, Batf3* ($n^{Xbp1fl/fl}$=5 mice, $n^{XBP1\Delta DC}$=3 mice). **c,** Level of eGFP expression in lung pre-DCs, cDC1s and cDC2s in mice harboring the 'late' *Cd11c*-Cre transgene (blue) or control mice (grey). Numbers in graphs represent percentage of eGFP$^+$ cells in one representative sample. Source data for suppl panel 2b can be found in Supplementary Table 2.

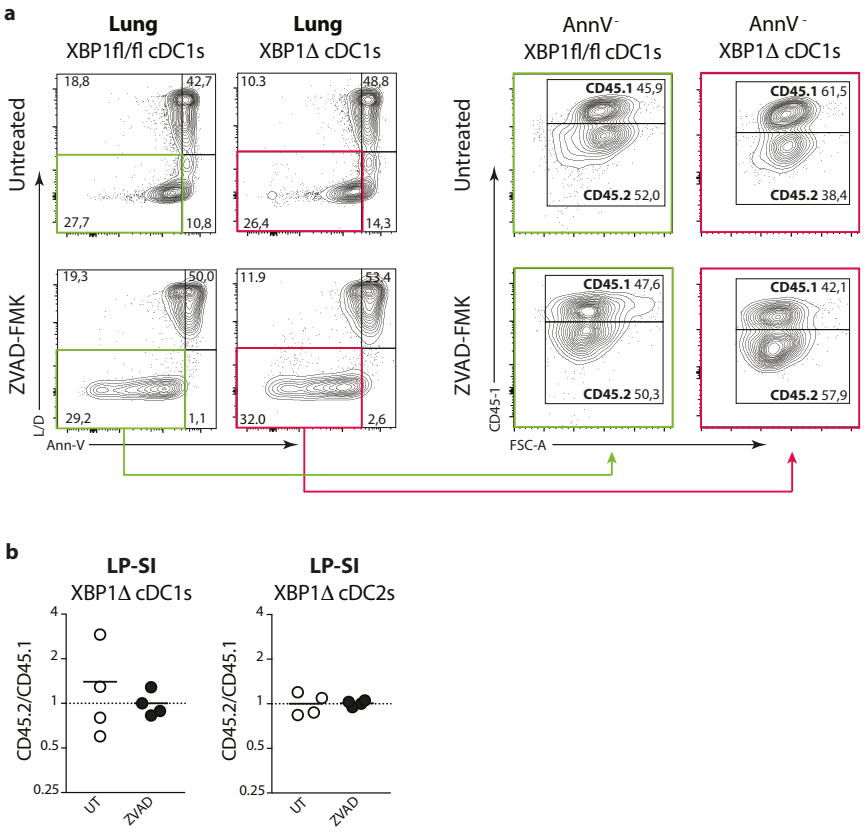

Supplementary Figure 4 Loss of XBP1 induces apoptosis in lung cDC1s. **a,** sorted lung CD45.2 cDC1 from *Xbp1*$^{fl/fl}$ or XBP1ΔDC origin mixed with CD45.1 counterparts and treated overnight with zVAD-fmk or vehicle. Cells were stained with Annexin-V and the DNA intercalator DAPI. Ratios of both CD45.2 *Xbp1*$^{fl/fl}$ and CD45.2 XBP1ΔDCs over CD45.1 WT counterparts (right panel) were determined within the non-apoptotic (Ann-V$^-$/DAPI$^-$) gate (left panel). Plots of one representative replicate are given. Depicted numbers are relative percentages. **b,** sorted LP-SI CD45.2 XBP1Δ cDC1 (top) and cDC2 (bottom) were mixed with CD45.1 counterparts and treated overnight with zVAD-fmk or vehicle. Ratio of Ann-V$^-$ cells is given. Each symbol represents 1 mouse. Mean ratio +/- S.E.M. is given. (n=4 mice). Source data for suppl panel 4b can be found in Supplementary Table 2.

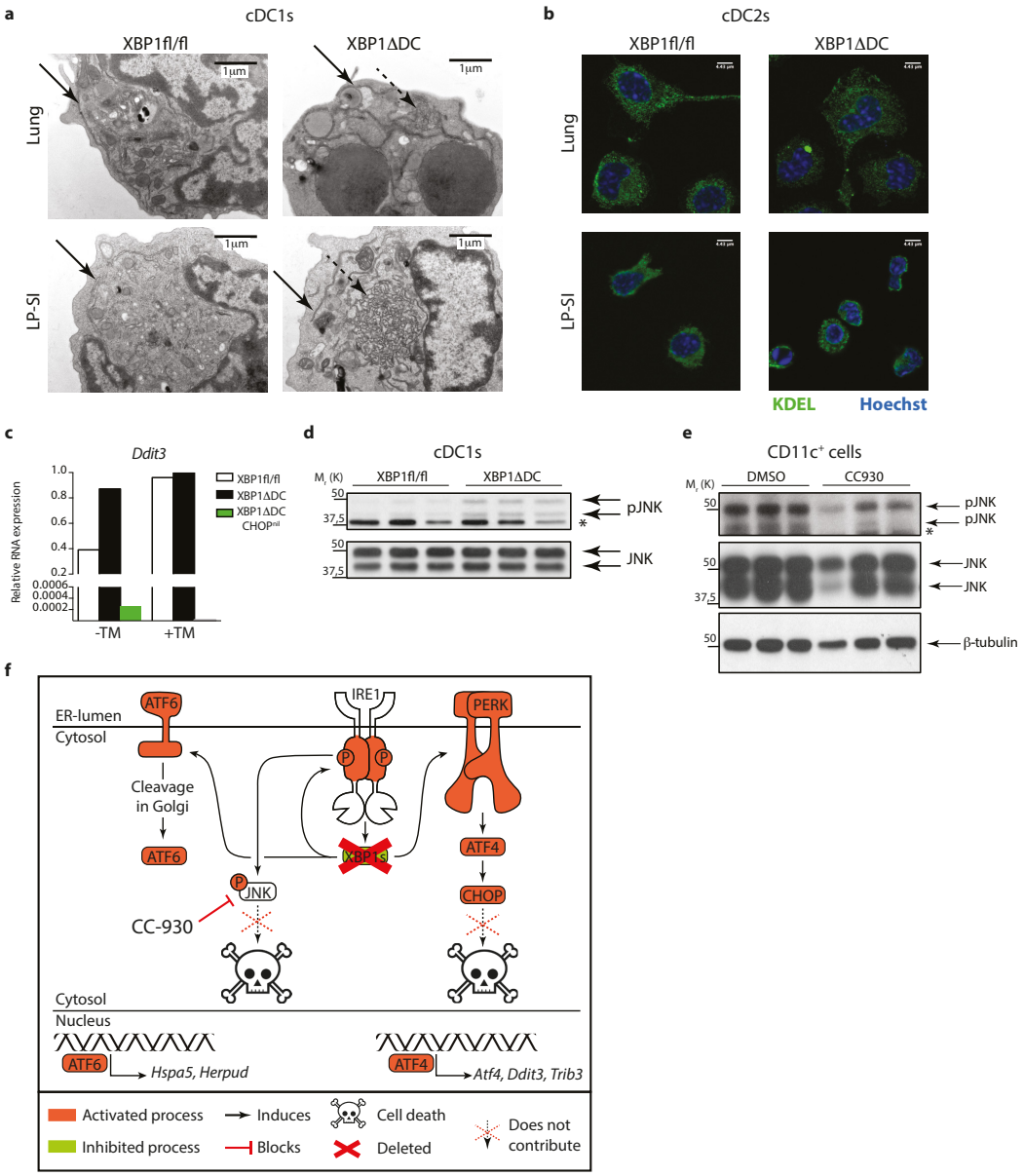

Supplementary Figure 5 ER stress induced death of cDC1 is CHOP and JNK independent **a,** transmission electron micrographs of FACS-sorted cDC1s and cDC2s derived from the lung or intestine of XBP1ΔDC or XBP1$^{fl/fl}$ mice. The full arrow indicates ER with normal appearance. The dashed line indicates an ER aggregate. Scale bars, 1 µm. **b,** immunofluorescence of cDC2s, sorted by flow cytometry from lung and LP-SI of *Xbp1*$^{fl/fl}$ and XBP1ΔDC mice, and stained with an anti-KDEL (ER-marker) antibody. Nuclei were stained with Hoechst. Scale bar: 4,43µm. **c,** RT-qPCR analysis of *Ddit3* mRNA among total RNA prepared from *in-vitro* cultured DCs. BM cells of *Xbp1*$^{fl/fl}$, XBP1ΔDC or XBP1ΔDC-CHOP^{nil} mice were cultured with GM-CSF and treated with tunicamycin (TM) or vehicle. Results are normalized to *gapdh* and *ywhaz*. Bar graph represents 1 sample. **d,** immunoblot analysis of phospho-JNK in flow cytometry sorted splenic cDC1s of XBP1fl/fl or XBP1ΔDC mice. Total JNK levels serve as loading control. Each lane represents one mouse. * indicates an aspecific band. **e,** immunoblot analysis of phospho-JNK of splenic XBP1ΔDC CD11c^{+} cells of XBP1ΔDC mice treated with CC-930 or vehicle. Total JNK and β-tubulin levels serve as loading control. Each lane represents one mouse. **f,** scheme illustrating activation of ATF6 and PERK branches ensuing XBP1 deletion in cDC1s. ATF6 and PERK activity resulted in enhanced transcription of target genes of both pathways. Loss of XBP1 also results into hyperactivation of IRE1 kinase activity and JNK phosphorylation. Nor CHOP (encoded by the *Ddit3* gene) nor JNK played a critical role in mediating cell death of XBP1Δ cDC1s in the lung.

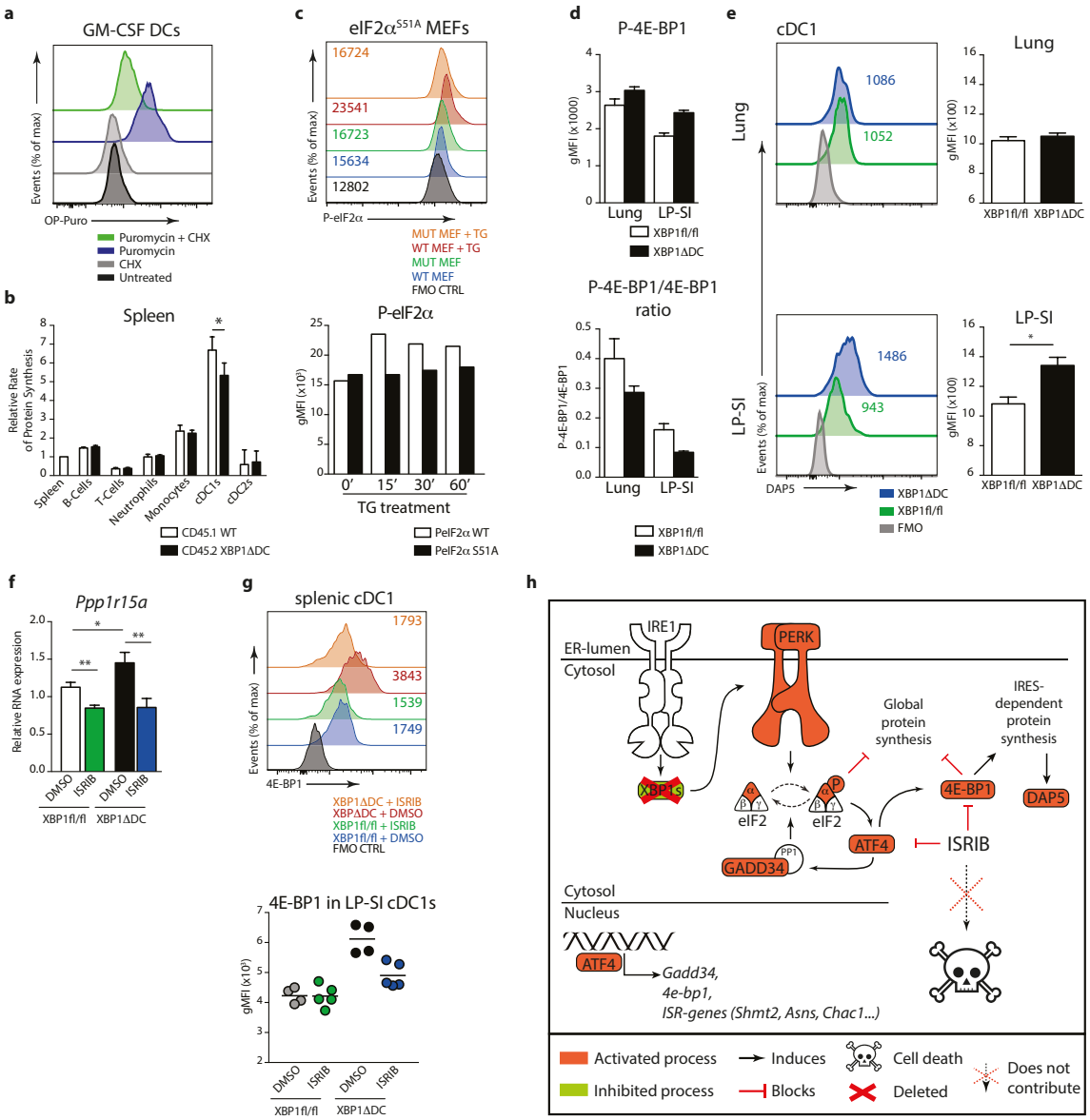

Supplementary Figure 6 Regulation of protein translation and integrated stress response in cDCs. **a,** histograms show fluorescence of OP-Puro incorporation in *in-vitro* cultured DCs, in presence or absence of the translation inhibitor cycloheximide (CHX). **b,** *in-vivo* OP-Puro incorporation in splenic cells after IP injection into CD45.1 wild type/CD45.2 XBP1ΔDC BM chimeric mice. Bar graphs represent mean protein synthesis rate +/- S.E.M. (n=6 mice). **c,** analysis of eIF2α phosphorylation in WT and eIF2α^{S51A} mutant MEFs upon thapsigargin treatment. Histograms and bar graphs depicting geometrical mean fluorescence are shown (n=1 experiment). **d,** phosphorylation status of 4E-BP1 in lung and intestinal cDC1s of *Xbp1*$^{fl/fl}$ and XBP1ΔDC mice. Ratio of phosphorylated P-4E-BP1 levels over unphosphorylated 4E-BP1 in lung and intestinal wild type versus XBP1ΔDCs. Bar graph shows mean +/- S.E.M. (n=5 mice). **e,** levels of DAP5 protein in lung and intestinal cDC1s of *Xbp1*$^{fl/fl}$ and XBP1ΔDC mice. Figures in histograms depict fluorescence of 1 representative sample. Bar graphs show mean fluorescence +/- S.E.M. P=0,0159, Mann-Whitney test (n=5 mice). **f,** RT-qPCR analysis of *Gadd34* RNA prepared from sorted splenic cDC1s of *Xbp1*$^{fl/fl}$ or XBP1ΔDC treated with ISRIB or vehicle. Results are normalized to *gapdh* and *b-actin*. Bar graphs represent mean +/- S.E.M. ($n^{Xbp1fl/fl\ DMSO}$=11 mice, $n^{XBP1fl/flDC\ ISRIB}$=8 mice, $n^{Xbp1\Delta DC\ DMSO}$=11 mice, $n^{XBP1\Delta DC\ ISRIB}$=10 mice). Unpaired Student T-test, $P^{(Xbp1fl/fl\ vs\ XBP1\Delta DC)}$=0,0483, $P^{(Xbp1fl/fl\ DMSO\ vs\ ISRIB)}$=0,0049, $P^{(XBP1\Delta DC\ DMSO\ vs\ ISRIB)}$=0,0039. **g,** histograms show fluorescence of 4E-BP1 in splenic cDC1s from *Xbp1*$^{fl/fl}$ and XBP1ΔDC mice treated with ISRIB or vehicle. Bar graph shows mean +/- S.E.M. of 4E-BP1 expression in intestinal cDC1s (n^{DMSO}=4 mice, n^{ISRIB}=5 mice). Data are representative of 1 (a,c) or 2 (b, d-g) independent experiments. Source data for panel 6g can be found in Supplementary Table 2. **h,** scheme illustrating ISR downstream of PERK. XBP1 deletion in cDC1s activates PERK, likely resulting into the (temporary) phosphorylation of eIF2α and ATF4 activation. ATF4 is a transcriptional regulator of *Gadd34*, *4ebp1* and several ISR target genes such as *Mtfhd2*, *Sesn2*, *Chac1*, *Mars*, *Asns*, *Shmt2* and *Gpt2*. Upon ATF4 mediated GADD34 expression, eIF2α is rapidly dephosphorylated again. However, protein translation inhibition is sustained in a 4E-BP1-dependent manner. 4E-BP1 engages IRES-dependent translation, leading to DAP5 induction. ISRIB blocks the PERK pathway preventing induction of ATF4 and 4E-BP1. However, despite inhibition of 4E-BP1, ISRIB did not trigger cell death.

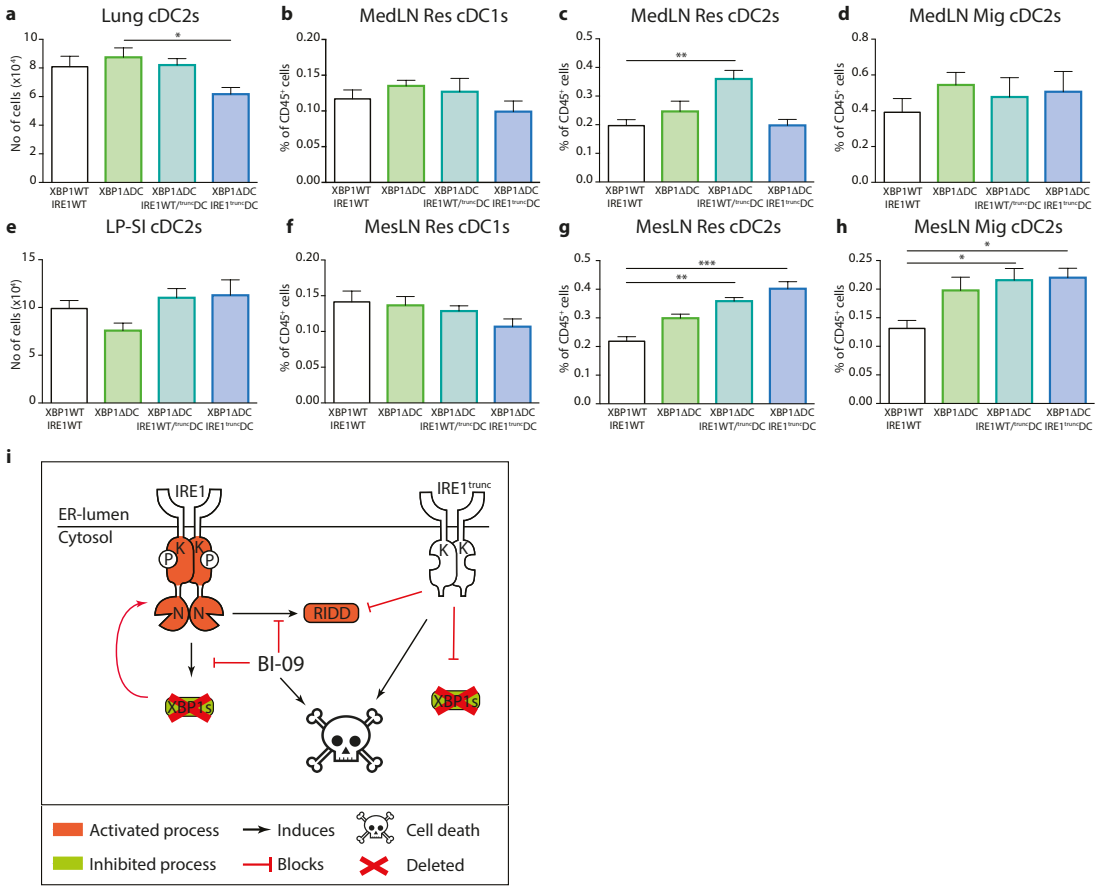

Supplementary Figure 7 RIDD activity promotes survival of XBP1 deficient intestinal cDC1s. **a,** no of lung cDC2s in XBP1/IRE1 WT, XBP1ΔDC, XBP1ΔDC/IRE1WT/^{trunc}DC and XBP1ΔDC/IRE1^{trunc}DC. Bar graphs represent mean +/- S.E.M. ($n^{XBP1/IRE1WT}$=13 mice, $n^{XBP1\Delta DC}$=8 mice, $n^{XBP1\Delta DC/IRE1WT/truncDC}$=7 mice, $n^{XBP1\Delta DC/IRE1truncDC}$=6 mice). Kruskal-Wallis test with Dunn's multiple comparisons. **b-d,** Percentage of resident cDC1s **(b),** resident cDC2s **(c),** migratory cDC2s **(d)** in the MedLN of XBP1/IRE1 WT, XBP1ΔDC, XBP1ΔDC/IRE1WT/^{trunc}DC and XBP1ΔDC/IRE1^{trunc}DC mice. Bar graphs represent mean percentage +/- S.E.M. ($n^{XBP1/IRE1WT}$=20 mice, $n^{XBP1\Delta DC}$=14 mice, $n^{XBP1\Delta DC/IRE1WT/truncDC}$=12 mice, $n^{XBP1\Delta DC/IRE1truncDC}$=5 mice). Kruskal-Wallis test with Dunn's multiple comparisons. **(e)** Number of intestinal cDC2s of XBP1/IRE1 WT, XBP1ΔDC, XBP1ΔDC/IRE1WT/^{trunc}DC and XBP1ΔDC/IRE1^{trunc}DC mice. Bar graphs represent mean +/- S.E.M. ($n^{XBP1/IRE1WT}$=13 mice, $n^{XBP1\Delta DC}$=8 mice, $n^{XBP1\Delta DC/IRE1WT/truncDC}$=7 mice, $n^{XBP1\Delta DC/IRE1truncDC}$=6 mice). Kruskal-Wallis test with Dunn's multiple comparisons. **f-h,** Percentage of resident cDC1s **(f)**, resident cDC2s **(g)**, migratory cDC2s **(h)** in the MesLN of XBP1/IRE1 WT, XBP1ΔDC, XBP1ΔDC/IRE1WT/^{trunc}DC and XBP1ΔDC/IRE1^{trunc}DC mice. Bar graphs represent mean percentage +/- S.E.M. ($n^{XBP1/IRE1WT}$=16 mice, $n^{XBP1\Delta DC}$=12 mice, $n^{XBP1\Delta DC/IRE1WT/truncDC}$=13 mice, $n^{XBP1\Delta DC/IRE1truncDC}$=11 mice). Kruskal-Wallis test with Dunn's multiple comparisons. *: p<0,05, **:p<0,01, ***:p<0,005. Data are pooled across 2 independent experiments. **i,** graphical scheme illustrating RIDD activation upon XBP1 deletion in cDC1s. Endonuclease activity of IRE1 was inhibited with complementary genetic (IRE1^{trunc}) and chemical (B-I09) approaches. Inhibition of RIDD induced cell death of chronically stressed cDC1s due to XBP1 deficiency.

Figure 7c

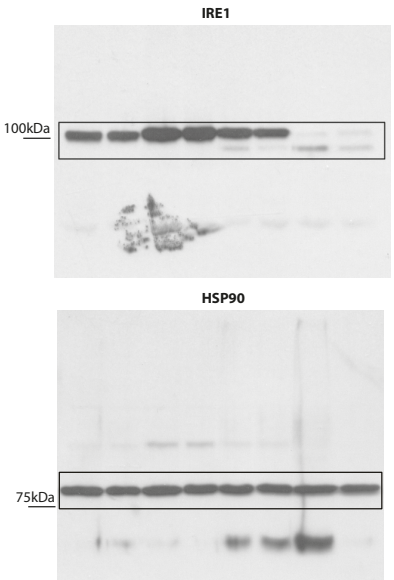

Supplementary Fig.5d

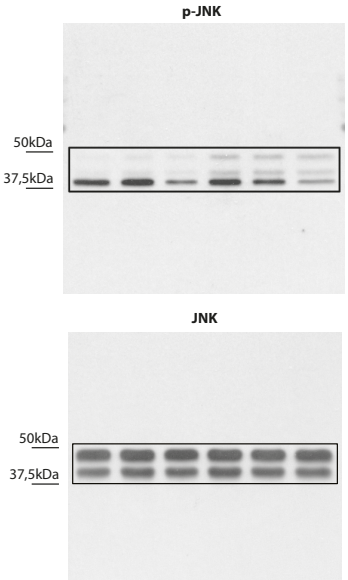

Supplementary Fig. 5e

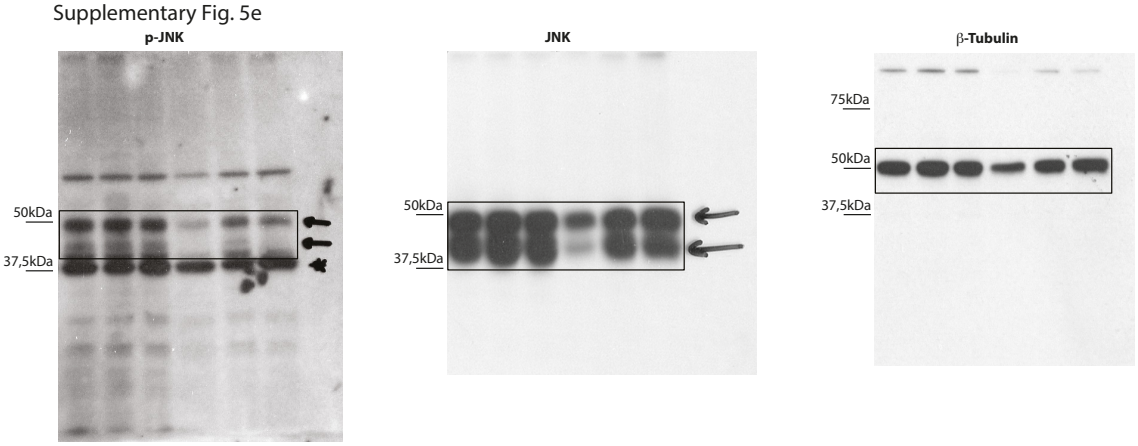

Supplementary Figure 8 Unprocessed scans of original western blots

Supplementary Table Legends

Supplementary Table 1 Used oligonucleotides. Sequences of all RT qPCR primers used in this study are provided.

Supplementary Table 2 Statistics source data. Raw data of the statistical analysis for experiments with n<5 replicates are provided.